J. Cosmet. Sci., **66,** 379–409 (November/December 2015)

Quantifying hair shape and hair damage induced during reshaping of hair

ROGER L. MCMULLEN, GUOJIN ZHANG,
and TIMOTHY GILLECE, *Ashland, Inc., Bridgewater, NJ 08807.*

Accepted for publication September 14, 2015.

Synopsis

The manipulation of hair shape, either to straighten or curl hair, is carried out on a grand scale in the hair care consumer market. Often, such changes are brought about through chemical or physical treatment, resulting in changes to hair chemistry. In this article, we review existing and present new data on methods to assess the efficacy of such treatments, mostly concentrating on imaging technologies used in conjunction with image analysis. In addition, we introduce spectroscopic imaging techniques and fluorescence spectrophotometry as tools to assess the biochemical state of the hair fiber as a result of hair shape modification regimens. Finally, we demonstrate how the structural integrity of the fiber is monitored with dynamic scanning calorimetry and traditional mechanical testing of the tensile properties of hair.

INTRODUCTION

As an outward expression of beauty, individuals often manipulate the shape of their hair to make themselves more attractive. Often, this involves subjecting hair to chemical and physical treatments that are carried out to change the shape of hair, such as permanent waving, relaxing, and hair straightening treatments (e.g., hot flat iron, Brazilian hair treatments, and Japanese straightening). Although permanent waving may be more of a niche market, relaxers are used almost universally by individuals with African hair, especially in the United States (1). In recent years, the use of hot straight irons and Brazilian hair treatments (e.g., Brazilian Blowout) has exploded (2). In order to gain a better grasp of the efficacy of products and treatments, it is desirable to have established techniques to quantify such changes in the three-dimensional geometry of the hair fiber assembly. One of the most suitable avenues for carrying out such analyses involves photographic imaging in combination with image analysis techniques (3). In most circumstances, these modifications to hair are accompanied by irreversible damage to the fiber's chemical and morphological structure. For example, thermal treatments carried out with hot irons can result in a loss of free and bound H_2O, tryptophan degradation, color changes, increases in mechanical combing forces, cuticle cracking (axial and radial), cuticle fusion and

Address all correspondence to Roger McMullen at rmcmullen@ashland.com.

bubble formation, and an increase in tensile strength (cross-linking). Such information was garnered from decades of research with both wool and hair (4–8). Chemicals treatments, such as permanent waving and hair straightening with relaxers, are also very damaging to hair. Typically, permanent waving is accomplished by treating the hair first with a reducing agent (e.g., mercaptoethanol) to break disulfide bonds, and then once hair is manipulated in the desired formation, it is treated with H_2O_2 to reform the disulfide links (9). As a result, the ensuing damage to permanently waved hair is paramount and leads to a reduction of the fiber's overall mechanical properties as well as surface damage. Commonly employed by individuals whose hair can be characterized as very tightly curled (e.g., African-type hair) or frizzy, hair straightening formulations (chemical relaxers) rely on the activity of strongly basic formulations that result in chemical and morphological changes in the hair shaft. Traditionally, NaOH-based (lye) relaxers were used to carry out such a task, resulting in a great deal of damage to the fiber including: disulfide bond cleavage, formation of lanthionine cross-links, supercontraction of the fiber, protein conformational changes (e.g., denaturation of the alpha-helical structure), and an increase in mechanical combing forces (10). More recently, lower pH chemical relaxers have been introduced into the market place; however, they still damage the fiber. In this article, we demonstrate the utility of imaging techniques for quantifying hair shape as well as state-of-the-art methods to monitor damage induced by treatments intended to reshape the hair.

IMAGING TECHINQUES AND IMAGE ANALYSIS TO QUANTIFY HAIR SHAPE

In the past decade, advances in photographic imaging have reached new heights, allowing scientists to gather data in pictographic form rather quickly and inexpensively. High-resolution images of hair are now easily generated by DSLR cameras with full exposure control that can be used in combination with sophisticated, yet economic, illumination systems. Another option for generating high-quality images is to utilize flatbed scanner technology. Some of the major advantages of scanners include reproducible light illumination as well as increased depth of field, both extremely applicable for examining hair tresses of varying shape. Regardless of the technique employed to generate images, data can be extracted from the photographs utilizing image analysis software, which is easily accessible for most laboratories. In the paragraphs that follow, we demonstrate the use of image analysis in combination with photographic techniques to measure the shape of hair. We are specifically interested in determining the amount of frizziness or curliness of hair as well as monitoring fiber alignment, which is extremely useful for measuring the straightening efficacy of a chemical relaxer or thermal styling treatment.

Morphological differences in various hair types lead to distinct geometries in the overall three-dimensional structure of the fiber assembly. In effect, we have a variety of hair shapes including: extremely fine to coarser grades of Caucasian hair of European descent, frizzy hair such as that of mulatto origin from Brazil, African hair types that tend to be extremely curly, hair from Middle Eastern countries and of Arabic descent, and Asian hair, which is probably a gross simplification of a selection of hair from distinct corners of this continent ranging from Japanese to Southern Indian and everything in between including a variety of Chinese hair types. Figure 1 contains photographs of a selection of hair types to illustrate the variety of fiber assembly shapes found in humans of different racial backgrounds.

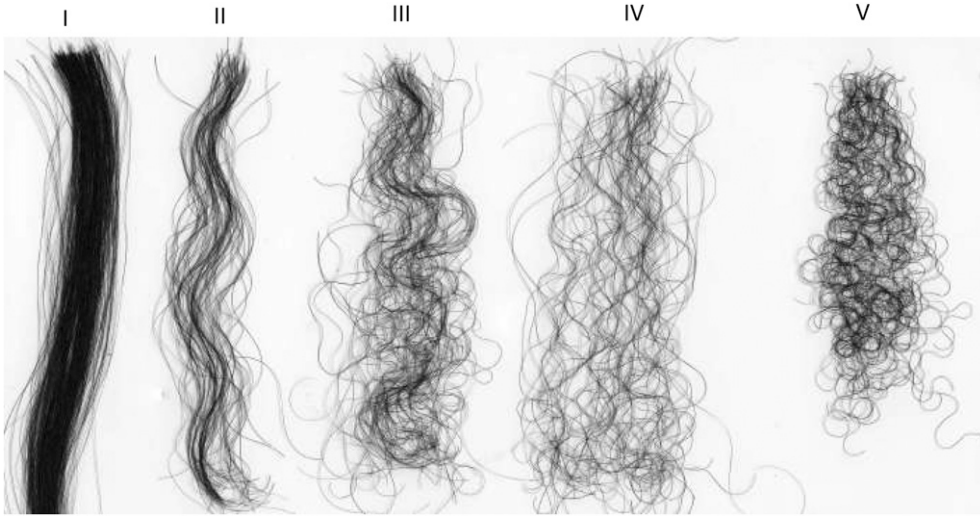

Figure 1. Images of various types of hair illustrating their diversity in shape. Type I is classified as straight European hair, Type II as wavy hair, Types III and IV as mulatto hair, and Type V as African-type hair.

MEASURING FIBER ORIENTATION BY TWO-DIMENSIONAL FOURIER TRANSFORM

Fiber alignment is a desirable trait for characterizing hair fiber assemblies since it defines the geometric arrangement of the fibers. For example, one may wish to quantify hair that has undergone permanent waving treatment to monitor changes in hair shape. Similarly, hair relaxer treatments are employed to eliminate the curl of hair. Thus, one may seek to quantify the degree of straightening induced by relaxer treatment. We may also wish to measure the de-frizzing or de-volumizing capacity of a treatment. These fiber assembly properties may be quantified using image processing techniques in combination with two-dimensional Fourier transform analysis.

In image processing, Fourier transform is used to remove repeating patterns from images, such as halftones from scanned images or periodic noise that can present itself in images obtained with certain instruments—these include transmission electron microscopy and scanning probe microscopies (11). Fourier transform may also be used to perform fractal analysis and to examine texture in images. Finally, it is also used to measure the orientation and alignment in images. Specifically, image transform techniques have found particular use in the quantification of fiber alignment of textiles (12).

Fourier transform decomposes an image from its spatial domain of intensities into a frequency domain with appropriate magnitude and phase values. In the frequency form of the image, gray scale intensities represent the magnitude of the various frequency components. Analysis is typically performed by using discrete Fourier transform:

$$F(u) = \frac{1}{N}\sum_{x=0}^{N-1} f(x)\mathrm{e}^{-\mathrm{i}2\pi ux/N} \qquad (1)$$

where N is the number of sampled points along the function $f(x)$, i is $\sqrt{-1}$, and $F(u)$ the transform function. It determines the rate at which an intensity transition occurs in a

given direction in the image. In the case of hair, if fibers are predominantly oriented in one direction, the spatial intensities in the perpendicular direction will be high.

As an example of fiber straightening, Figure 2 contains images of African hair in its native state (A) and at increasing levels of relaxer treatment (B and C). Visual observation clearly reveals the change in fiber curvature when comparing untreated hair with partially (B) and fully (C) relaxed hair. The corresponding two-dimensional Fourier transform images are shown adjacent to the original images of hair and provide us with a measure of fiber alignment. In the case of untreated African hair, there is no directionality apparent in the transformed image. The Fourier transform distribution is omnidirectional. However, when we examine the partially relaxed hair sample, a more narrow distribution appears demonstrating that fibers are beginning to exhibit a repeating pattern. In the fully relaxed hair, the distribution becomes even more narrow and intense, indicating fiber alignment along a principle axis. Since the Fourier transform images are symmetrical, only half of the image needs to be quantified. A 180° arc is drawn circumferentially from one axis of the Fourier transform image to another, allowing us to measure light intensity (luminosity) along the arc. From the plot of luminosity versus arc angle, we observe a peak corresponding to fiber alignment distribution. In the case of untreated African hair, the peak is very wide (177°); however, the partially and fully relaxed hair samples had peak widths of 35° and 18°, respectively. In this case, we demonstrate the utility of two-dimensional Fourier transform analysis for characterizing relaxer treatments of African hair. It may also be applied to quantifying other chemical or physical treatments of hair, thereby resulting in geometrical changes of the fiber assembly, or even to characterize hair styling configurations such as brading.

HAIR CURLINESS

It is often desirable to measure the degree of hair curliness to evaluate the efficacy of cosmetic treatments, or just to investigate the curliness of a given hair type. Using a method proposed by Loussouarn and coworkers, the length of the hair is measured at rest, then fully stretched, to calculate the curl index (CI) (13):

$$CI = \frac{Length_{rest}}{Length_{stretched}} \qquad (2)$$

In the original method, fiber measurements are conducted without the aid of image analysis or imaging equipment. In this study, we obtain images of hair with a flatbed scanner, which is calibrated with a measuring scale. Images of three hair types, African, artificially curled, and frizzy, are provided in Figure 3. Representative fibers are shown in the relaxed and stretched state. Applying Equation 1 to the distance measurements yields curl indices of 2.25 ± 0.15, 1.58 ± 0.16, and 1.19 ± 0.24 for African, artificially curled, and frizzy hair, respectively. These data represent an average of measurements for five fibers of each hair type.

HAIR VOLUME

The volume of a hair fiber assembly can be measured with great facility using a three-dimensional laser stereometer (14). Such a device can be constructed utilizing an x-y

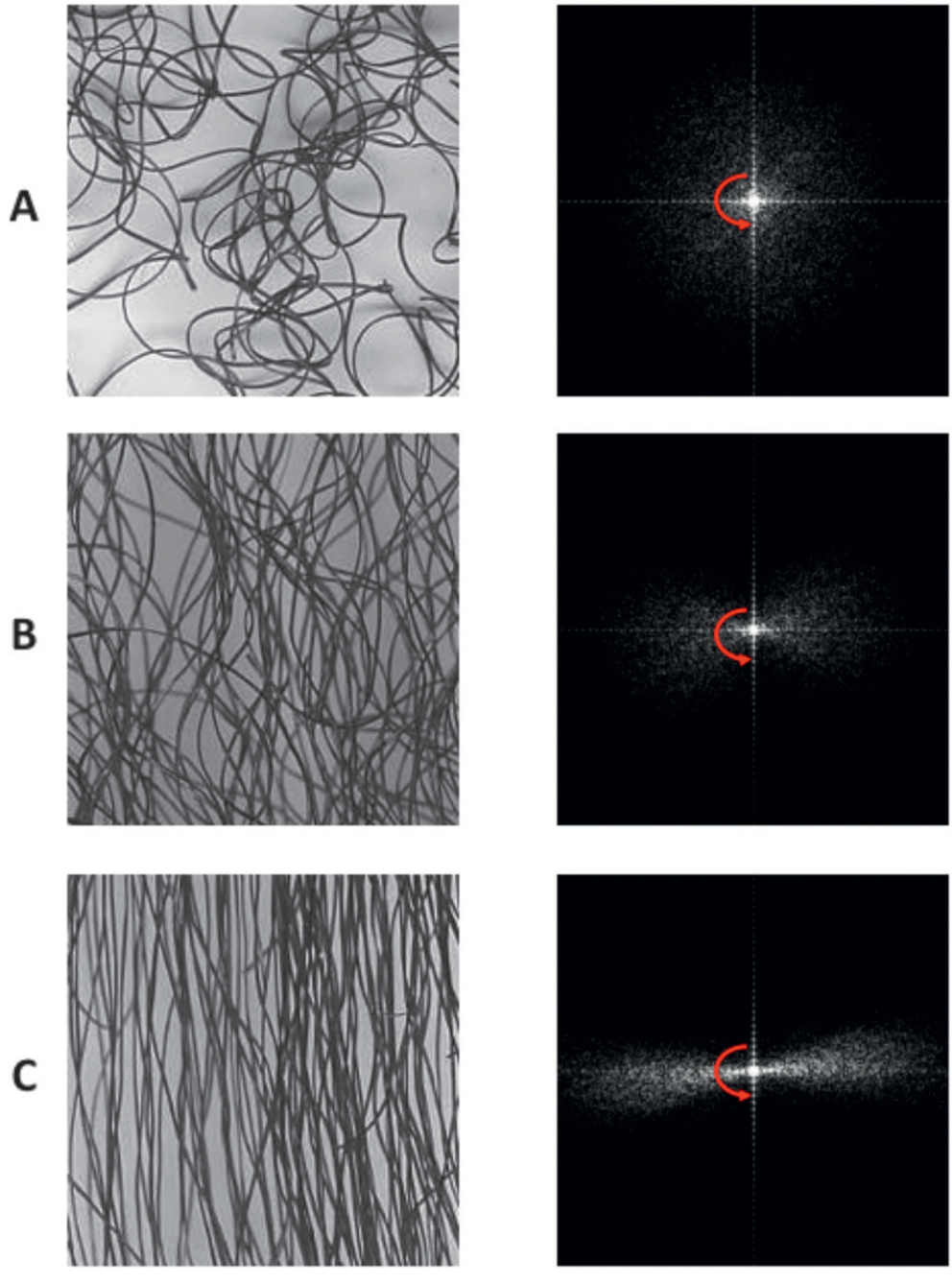

Figure 2. Images and their corresponding two-dimensional Fourier transform for (A) untreated African hair and the same hair type that underwent a (B) partial and (C) full chemical relaxation procedure.

two-dimensional translational stage and a laser device, which provides distance information in the z direction. The distance data are obtained by triangulation of the reflecting red laser beam from the surface of the measured object, in this case hair. Since hair fiber

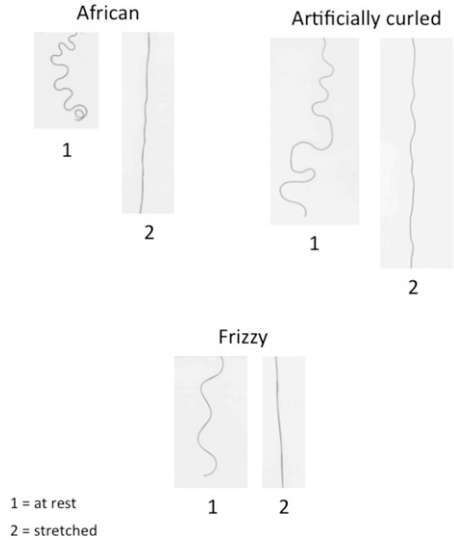

Figure 3. Images of hair with various degrees of curvature in the relaxed and fully extended states.

assemblies do not have a continuous solid surface, each z-dimension reading is an average of measurements obtained from multiple reflections corresponding to fibers at various depths below the outermost hair surface. The utility of this technique lies in its ability to measure changes in the volume of hair tresses subjected to chemical or physical treatment intended to reshape hair. Utilizing this approach, a hair tress may be positioned on the platform of the translation stage and a surface plot corresponding to the three-dimensional volume occupied by the hair assembly may be constructed. In addition, data are also presented in the form of contour plots or cross-sectional representations of the hair tress allowing one to view the tress along its primary axis. As an example of the technique relevant to reshaping hair, Figure 4 contains images and three-dimensional plots of virgin frizzy hair and the same hair that underwent a hair straightening treatment. In both the images and the contour plots, it is clearly evident that a reduction in the overall volume of the tress occurs due to reduction of frizz. Regardless of the reshaping procedure employed, laser stereometry provides a useful modality for monitoring three-dimensional shape and volume occupied by a hair fiber assembly.

SPECTROFLUORESCENCE TECHNIQUES TO CHARACTERIZE BIOCHEMICAL CHANGES IN HAIR

Steady-state spectrofluorescence is a useful tool to monitor the health of biological tissues as it can measure the level of tryptophan (Trp), which is representative of protein integrity. In addition to Trp fluorescence, several other fluorophores are also present in hair and are believed to be attributed to kynurenenine, N-formylkynurenine, and 3-hydroxykynurenine, which are known metabolic and degradation products of Trp that are affected by environmental stresses normally experienced by hair (15). Nowadays, we are able to construct an endogenous fingerprint of fluorescent compounds present in hair by employing a range of excitation wavelengths from 270 nm to 450 nm with a resolution of 2 nm.

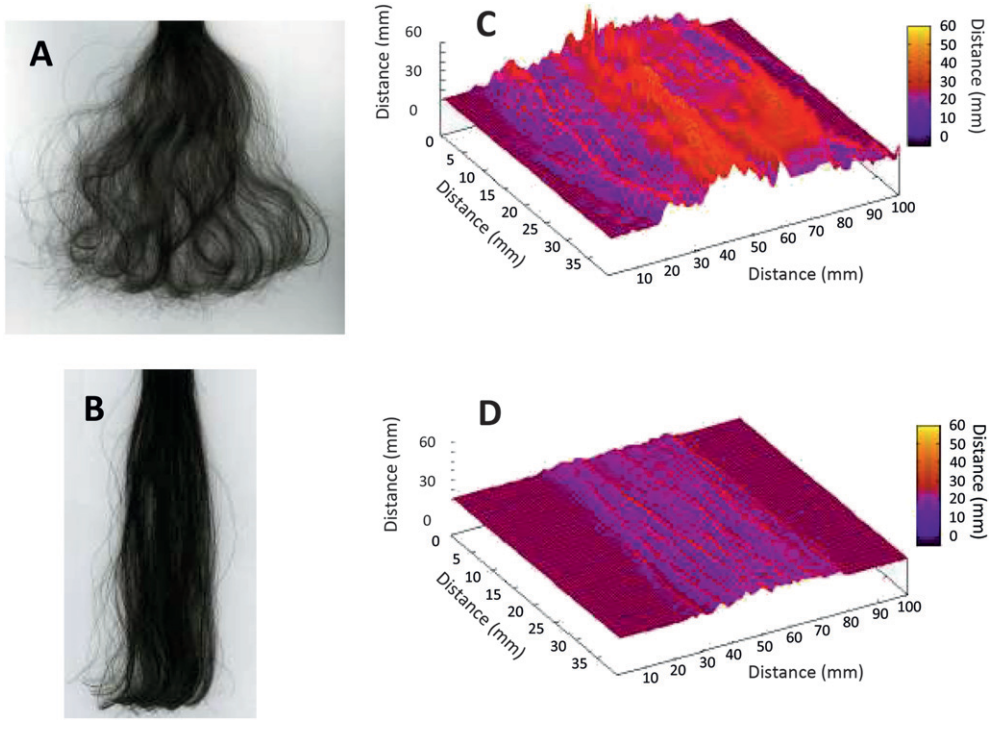

Figure 4. Images and three-dimensional plots of (A and C) virgin frizzy hair and the same hair that underwent a hair straightening treatment (B and D).

As a result, we can generate surface plots of fluorescence emission as a function of excitation and emission wavelengths (excitation–emission matrices). Thus, we are able to profile the levels of various structural molecules in hair before and after exposure to thermal straightening irons as well as to chemical treatments such as permanent waving systems or relaxers.

SPECTROFLUORESCENCE BACKGROUND

Previous studies of the intrinsic fluorescence of hair yielded information about the effects of chromophores on the fluorescent behavior of Trp and its metabolic/degradation products: kynurenenine, N-formylkynurenine, and 3-hydroxykynurenine (15). The effects of melanin on the fluorescence of these molecules can be monitored by comparing highly pigmented dark brown hair with nonpigmented Piedmont hair or white hair. Piedmont hair contains higher levels of yellow pigmentation than pure white hair. Gray hair may also contain yellowish coloration, presumably present due to exposure to ultraviolet (UV) radiation, which is believed to be attributed to higher levels of 3-hydroxykynurenine (16). In general, hair containing greater quantities of melanin has much lower emission characteristics, most likely because more light absorbed by melanin will result in less light available to interact with Trp and other fluorophores. Further, Trp fluorescence is highly dependent on the moisture content of hair, with greater Trp fluorescence occuring

at higher levels of hydration (15). Trp fluorescence is known to be extremely sensitive to its immediate environment, and may increase or decrease depending on the mobility of the Trp residues. One may even observe an increase in Trp fluorescence when hair is subjected to damaging treatments such as permanent waving due to the cleavage of disulfide bonds. Although one may expect less Trp to be present after such a damaging treatment, such an effect may be explained by an increase in the mobility of Trp residues in the protein in the absence of disulfide bonds (17).

In hair, we observe several distinguishable fluorescence peaks when examining the spectrofluorescence excitation–emission matrices. Trp is the most familiar with an excitation wavelength of 290 nm and an emission maximum between 335 and 345 nm, depending on the degree of pigmentation—the greater the pigmentation, the longer the wavelength of the peak maximum. In previous studies, we identified several emission peaks in the UVA–visible region that could be attributed to Trp metabolic/degradation products, including N-formylkynurenine, kynurenine, and 3-hydroxykynurenine (15). Figures 5 and 6 provide excitation–emission matrices for dark brown and Piedmont (white) hair. The difference in melanin content between these two samples greatly affects the spectrofluorescence thumbprint. In dark brown hair, the Trp peak (I_{ex} = 290 nm, I_{em} = 343 nm) appears as a minor constituent next to the large conglomerate of the kynurenines (I_{ex} = 366 nm, I_{em} = 433 nm). Such a greater fluorescence emission in the case of the kynurenines may be attributed to either higher concentration of these fluorophores or less quenching by melanin (as compared to Trp where melanin absorption is greater). In the case of Piedmont hair (Figure 6), the Trp peak appears to be barely present (I_{ex} = 292 nm, I_{em} = 337 nm) due to its miniscule emission relative to the kynurenines (I_{ex} = 378 nm, I_{em} = 448 nm). More than likely, this is an optical effect in which case less melanin allows much greater fluorescence for all fluorophores in the tissue. Melanin has a monotonically decreasing absorption spectrum when going from shorter to longer wavelengths. Contrary to intuition, it appears to influence the fluorescence of the kynurenines to a greater extent than Trp.

In the sections below, we compare peak intensities for Trp and the kynurenines from virgin hair with those of hair subjected to damaging treatments. We report the intensity of Trp, the kynurenines, and a degradation product of the kynurenines (I_{509}). We also examine the ratio of these peaks to better understand the effects of these treatments on protein degradation.

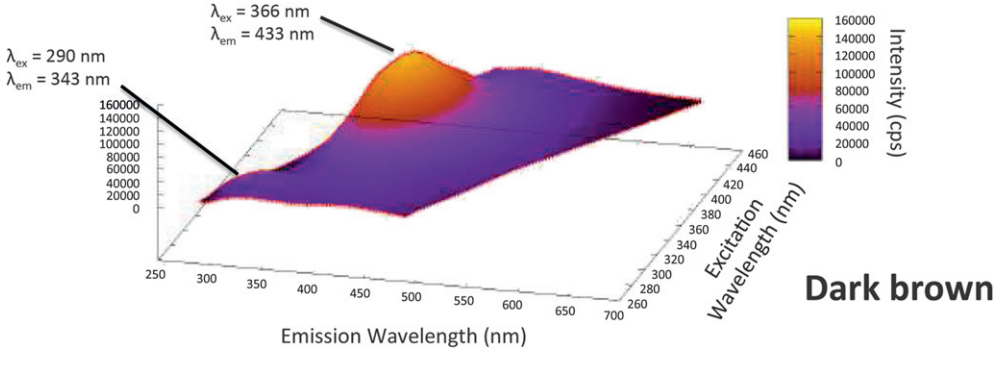

Figure 5. Spectrofluorescence excitation-emission matrix of dark brown hair.

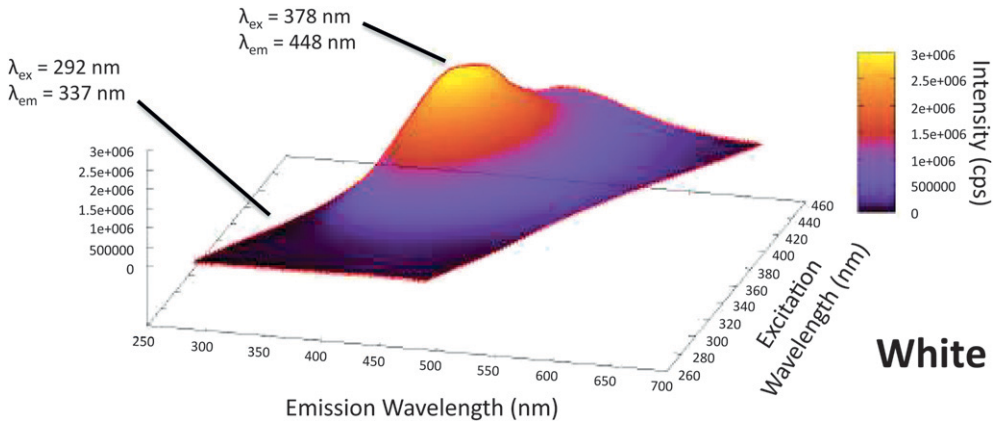

Figure 6. Spectrofluorescence excitation-emission matrix of Piedmont hair.

THERMAL DEGRADATION OF HAIR

Frequently, hair is exposed to thermal treatments to provide a desired hair set or style. In previous studies, we found that hair experiences surface (cuticular) and internal (cortical) damage as a result of thermal treatment (7). Hair also undergoes color changes on exposure to heat. This is clearly evident in the photograph of Piedmont hair shown in Figure 7, where one can visually observe the region of the tress where the hot iron treatment was administered, resulting in the formation of a dark yellow hue. In the case of dark brown hair, we do not observe a visually significant color change, probably because it is masked by the absorption of melanin. Thermal treatment was administered for 1 min of

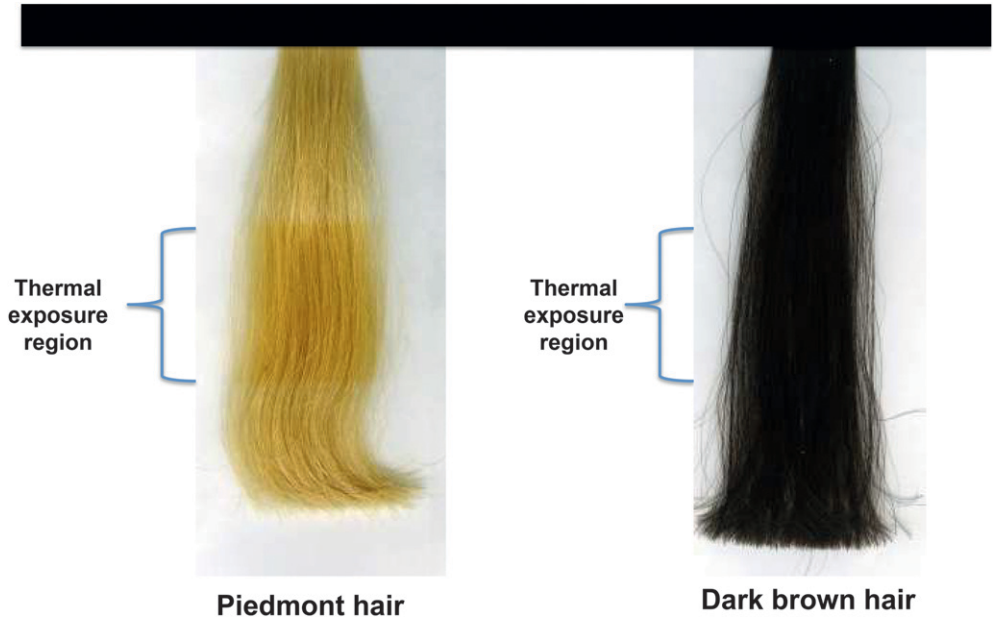

Figure 7. Photographs of thermally exposed Piedmont and dark brown hair.

continuous treatment. For this particular hot iron application, such a length of treatment might be considered extensive. However, this time scale was meant to be representative of cumulative treatments (i.e., a summation of a series of short treatment protocols) providing an overall equivalent treatment time to the continuous treatment. In fact, previous studies show that cumulative treatment is actually more damaging than continuous treatment (7).

Data extracted from the excitation–emission matrices for thermally treated Piedmont and dark brown hair are provided in Table I. For dark brown hair, we observe a decrease in the residual Trp levels while the I_{Kyn} and I_{509} bands are statistically similar when comparing the thermally exposed region of the tress with the unexposed portion. The calculated peak ratios reveal the same information. In Piedmont hair, thermal exposure results in Trp loss, degradation of kynurenines, and an increase in the intensity at I_{509}. As expected, the ratio, I_{Trp}/I_{Kyn}, decreases in thermally exposed hair as compared to the unexposed region of the tress. In contrast, there is an increase in I_{509}/I_{Kyn} in thermally exposed Piedmont hair. We suspect that the observed increase in this ratio is due to the formation of yellow coloration in thermally exposed hair.

HAIR STRAIGHTENING

The peak intensities and ratios for chemically relaxed hair are provided in Table II. As a result of the relaxer treatment, Trp fluorescence decreases for both dark brown and Piedmont hair (compared to untreated readings in Table I). In contrast, the signal for I_{Kyn} is essentially the same as for untreated hair in both dark brown and Piedmont hair. Although Trp degradation to kynurenines may occur—which would lead one to expect an increase in I_{Kyn}—the kynurenines themselves may be degraded by the relaxer treatment. In the case of the peak at the highest excitation wavelength employed, resulting in emission at I_{509}, relaxer treatment results in a large decrease in peak intensity for Piedmont hair and no change for dark brown hair. This effect may be more pronounced for Piedmont hair since its fluorescence in this region is much more discernible. The peak ratios are also provided in Table II, which correspond with the peak intensity observations.

INFRARED SPECTROSCOPIC IMAGING TO MONITOR LIPID DISTRIBUTION AND PROTEIN CONFORMATION IN HAIR

Infrared (IR) spectroscopy is an indispensable tool for the study of biological samples due to the inherent chemical specificity of vibrational frequencies in the IR spectrum. By coupling an FT-IR spectrometer with a microscope, one may perform FT-IR spectroscopic imaging, which allows for the measurement of the chemical environment of a specific area of a specimen. In this way, we can spatially resolve molecular structure information. In essence, a two-dimensional matrix, composed of pixels, contains an IR spectrum in each pixel. This allows us to generate FT-IR images corresponding to a chosen vibration frequency of interest.

In the past two decades, FT-IR spectroscopic imaging has transformed into a powerful biophysical approach to study various types of biological tissues (18–21). The spatially resolved spectroscopic images generated from this technique provide a histological map

Table I
Peak Intensity Values and Pertinent Peak Ratios for Dark Brown and Piedmont Hair Exposed to Thermal Treatment. Data are Provided for the Unexposed and Exposed Regions of the Hair Tress

	I_{Trp}	I_{Kyn}	I_{509}	I_{Trp}/I_{Kyn}	I_{509}/I_{Kyn}
Dark brown	24,550 ± 2,616	103,050 ± 5,586	33,250 ± 7,283	0.239 ± 0.038	0.321 ± 0.053
Dark brown-thermal	15,100 ± 849	108,000 ± 4,243	29,650 ± 4,172	0.140 ± 0.002	0.276 ± 0.049
Piedmont	44,600 ± 5,657	2,030,000 ± 98,995	1,275,000 ± 63,640	0.022 ± 0.001	0.621 ± 0.062
Piedmont-thermal	18,900 ± 1,838	1,800,000 ± 127,279	1,540,000 ± 28,284	0.010 ± 0.000	0.858 ± 0.076

Table II
Peak Intensity Values and Pertinent Peak Ratios for Dark Brown and Piedmont Hair Exposed to Chemical Relaxer Treatment. Compare These Data with the Untreated Values (Dark brown and Piedmont) in Table I

	I_{Trp}	I_{Kyn}	I_{509}	I_{Trp}/I_{Kyn}	I_{509}/I_{Kyn}
Dark brown-relaxer	19,150 ± 636	108,000 ± 2,828	26,650 ± 1,061	0.177 ± 0.001	0.247 ± 0.003
Piedmont-relaxer	26,150 ± 1,485	2,155,000 ± 35,355	728,700 ± 28,284	0.012 ± 0.000	0.672 ± 0.002

of the endogenous biochemical components (proteins, lipids, DNA, etc.) within a tissue section without the use of stains or probes. In addition, the vast amount of data inherent in spectral imaging permit sophisticated multivariate analyses such as cluster, principal component, and factor analyses, which enhance the ability to detect altered spatial regions in a heterogeneous sample. Combining univariate analysis and multivariate techniques provides a unique spectral-structure correlated characterization of biological samples.

It has been known for some time that traditional FT-IR spectroscopy is a useful tool for quantifying oxidative damage in hair (22). More recently, FT-IR spectroscopic imaging has been very effective at examining the spatial distribution of specific biological molecules in hair on the morphological level (23–25). In this section, we demonstrate the ability of these techniques to generate spatially resolved images of hair chemistry, anatomy, protein distribution, and protein secondary structure information. It can also be employed to map lipid distribution and the conformation in hair.

INTERPRETATION OF SPATIALLY RESOLVED FT-IR SPECTRAL IMAGES

Utilizing cross sections of human hair, one can map and monitor protein conformation in the morphological sections of the fiber. Figure 8A contains an optical micrograph of several hair fiber cross sections, which were subject to FT-IR spectroscopic imaging. The FT-IR image in Figure 8B was generated by extracting the waveband intensity information from FT-IR spectra (from each pixel in the matrix) at 1650 cm^{-1}, which approximates the amide I band corresponding to the protein backbone and identifies the type of secondary structure (see paragraph below with reference to the band at 1652 cm^{-1}). In one of the hair fiber cross sections in that image (upper right side), three white pixels are provided as indicators where the spectra shown in Figures 9A, 9B, and 10 were obtained. In Figure 9A, Amide I and II bands are clearly evident in the three major morphological components. These bands, which arise between 1480 and 1750 cm^{-1}, correspond to molecular vibrations in the backbone of keratin protein and are indicators of the secondary structure, whether it be alpha helix or beta sheet, or random coil (26). In the cortex and medulla, both peaks are sharp and their position is indicative of alpha-helical conformation. On the other hand, spectra from the cuticle are much broader and point to a greater presence of beta sheets in its structure. Figure 9B contains spectra obtained at 2800–3700 cm^{-1} and correspond to symmetric (2850 cm^{-1}) and asymmetric (2924 cm^{-1}) C–H stretching in the methylene groups of lipids. Another band at 2960 cm^{-1} is due to C–H stretching in methyl groups of proteins. By taking the peak area ratio of 2850 to 2960 cm^{-1}, we can determine a relative level of lipids in the hair cross sections.

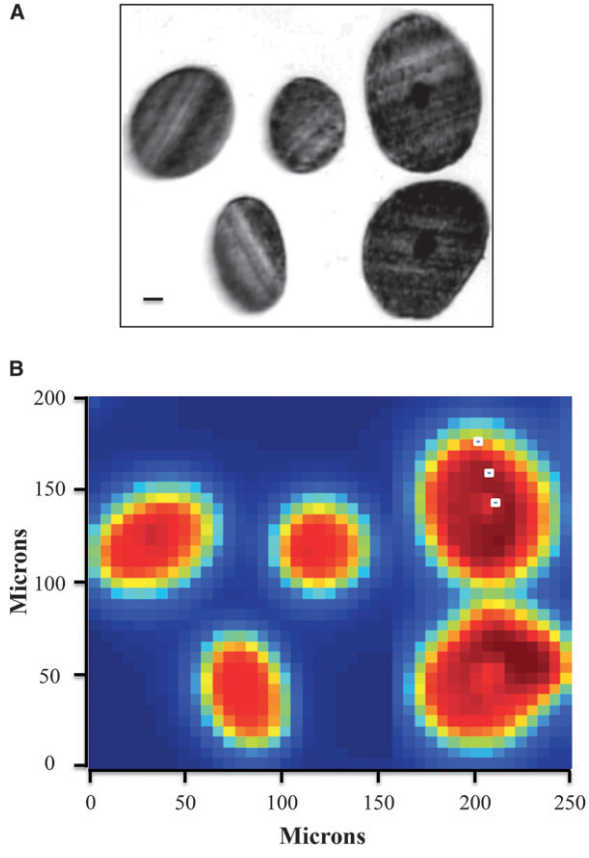

Figure 8. (A) Optical micrograph and (B) FT-IR spectroscopic image of cross sections of dark brown hair. The calibration bar in (A) is equivalent to 20 µm. Spectra for the three white pixels—corresponding to cuticle, cortex, and medulla—in the cross section in the upper right corner of the (B) FT-IR image are shown in Figures 5 and 6. Originally published in Reference 25. Reprinted with permission of the Society of Photo Optical Instrumentation Engineers, Copyright 2011.

By conducting second derivative order analysis of the spectra in Figure 9A (see Figure 10), it is much easier to resolve other bands in the amide region to gain further insight into the secondary structure of the protein. Amide I and II bands at 1652 and 1548 cm^{-1} correspond to the presence of alpha keratin while amide I bands at 1630 and 1695 cm^{-1} and an amide II band at 1516 cm^{-1} suggest antiparallel beta sheet conformation (20,27). Many of the investigated treatments result in the conversion of alpha keratin to beta keratin, which can be in the parallel or antiparallel conformation. On the basis of this data, one may generate FT-IR images where the intensity ratio of 1516 cm^{-1} to 1548 cm^{-1} is representative of beta sheet conformation relative to alpha-helical structure. Thus, in the image shown in Figure 10 each pixel represents this ratio and higher levels of beta sheet conformation correspond to brighter colors (red/orange) in the image while darker colors (bluish) indicate lower levels of beta sheets (higher alpha keratin). As illustrated in the figure, the proteins of the cuticle tend to be predominantly in the beta sheet conformation, whereas the cortex and medulla are dominated by proteins with alpha-helical structure.

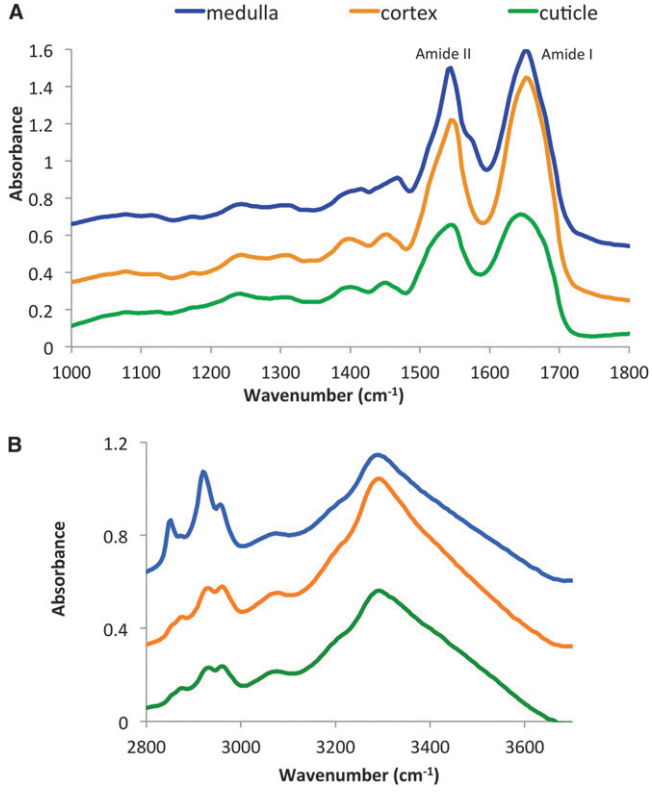

Figure 9. Infrared spectra for the white pixel regions in Figure 8B sampled from the cuticle, cortex, and medulla. (A) Spectra in the 1000–1800 cm^{-1} region of the infrared spectrum corresponding to amide I (1652 cm^{-1}) and II (1648 cm^{-1}) bands. (B) Spectra in the 2800–3700 cm^{-1} region of the infrared spectrum illustrating the symmetric (2850 cm^{-1}) and asymmetric (2924 cm^{-1}) stretching of C–H bonds in the lipid methylene groups and C–H bonds in lipid methyl groups (2960 cm^{-1}). The peak at 3300 cm^{-1} in (B) is assigned to N–H stretching in protein. See text for further explanation. Originally published in Reference 25. Reprinted with permission of the Society of Photo Optical Instrumentation Engineers, Copyright 2011.

MONITORING PROTEIN CONFORMATION IN THERMALLY EXPOSED HAIR

Thermal exposure of hair results in surface and internal damage to its structure. This is not surprising since many commercially available thermal styling devices can reach temperatures as high as 230°C, well beyond the denaturation temperature of alpha keratin and reaching its melting point. Not surprisingly, and based on the discussion in the previous section, FT-IR spectroscopic imaging is perfectly suited for studying changes in protein conformation brought about by thermal treatments. A detailed look at hair fiber cross sections exposed to a flat iron at a temperature of 230°C for 12 min is provided in Figure 11 (Please note that this was a treatment regimen consisting of 12 s per pass with the flat iron on a hair tress for a total cumulative treatment time of 12 min). This FT-IR spatially resolved spectroscopic image was generated by taking the peak intensity ratio of spectroscopic bands at 1516 cm^{-1} to 1548 cm^{-1}. (The reader should note that the second derivative curves are used to identify the peak positions; however, intensity ratios are taken from the original spectra.) Hence, the resulting FT-IR image provides a measure of the level of beta keratin present in the specimen (with blue corresponding to low levels and

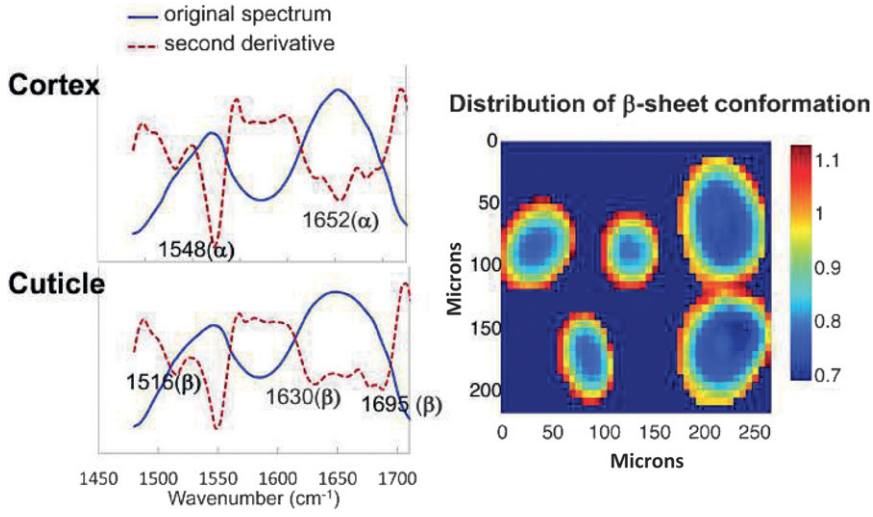

Figure 10. Spectra in the amide region of the infrared spectrum for the cuticle and cortex indicative of alpha (1548 and 1652 cm^{-1}) and beta (1516, 1630, and 1695 cm^{-1}) conformation of hair proteins. See text for peak assignments. Also, an accompanying FT-IR image based on the peak intensity ratio of 1516 to 1548 cm^{-1} obtained from the spectra, illustrating the level of beta sheet present in the cross sections. Higher levels of beta sheet are found in the cuticular region of hair. Originally published in Reference 25. Reprinted with permission of the Society of Photo Optical Instrumentation Engineers, Copyright 2011.

red/orange/yellow to higher levels). In virgin hair, as already noted in the section above, we find greater quantities of proteins in the beta conformation in the cuticular region than in the cortex or medulla. However, after exposure to elevated temperatures the amount beta keratin increases significantly in the cortex as evidenced by the decrease in dark blue color in this region. Such a result is in accordance with thermal degradation studies of hair by dynamic scanning calorimetry (DSC) (28,29). We observe similar effects when hair is treated with alkaline solution (0.1% NaOH), which is comparable to exposure experienced by the consumer during hair relaxer treatment.

RAMAN SPECTROSCOPIC IMAGING TO MEASURE LIPID CONFORMATION AND ORDER AND DISULFIDE BOND DISTRIBUTION

Raman confocal imaging is a complementary spectroscopic technique to FT-IR spectroscopy and can provide additional information about the molecular structure and chemistry of the hair fiber. It has much greater spatial resolution than FT-IR imaging, and with confocal capabilities can noninvasively (does not require physical sectioning) generate information about the external and internal morphological components of the fiber. Typically, Raman confocal imaging operates in two distinct data collection modes: X-Y lateral sectioning (surface scan) or X-Z cross sectioning (depth profiling). In the surface scan mode, one can generate a matrix of spectra (similar to FT-IR imaging) that corresponds to a selected plane in the sample. Depth profiling, on the other hand, refers to collection of spectra along a Z-line at various depths in the tissue. In either case, the sample is irradiated with a laser (e.g., 785 nm) and the resulting Raman spectra are recorded utilizing a Raman spectrometer coupled with a confocal microscope. Like IR, Raman spectroscopy provides

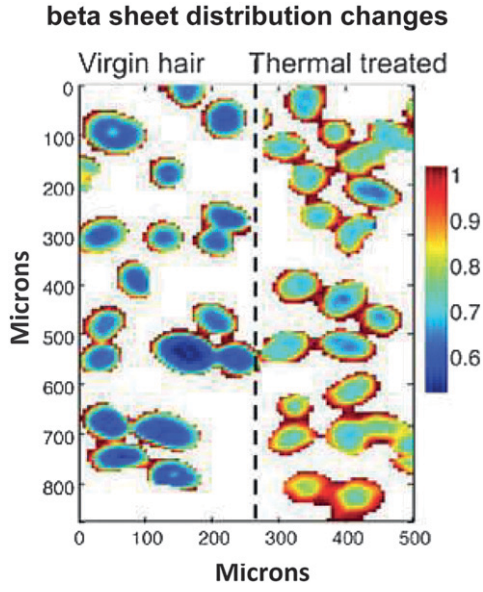

Figure 11. FT-IR image and representative spectra illustrating beta sheet distribution in virgin and thermally treated hair. The FTIR image was generated from the peak intensity ratio of 1516 to 1548 cm^{-1} obtained from the spectra gathered for each pixel. The representative spectra were obtained from European dark brown hair.

molecular vibrational information about the sample. However, Raman information is based on scattering (rather than absorption) and often contains more detailed information (less broad peaks) allowing for better discrimination between constituents in the sample.

ASSIGNMENT OF BANDS IN RAMAN SPECTRA OF HAIR

Figure 12 contains a series of Raman spectra that were obtained in depth profiling mode (2 μm steps) for a human hair fiber beginning at the surface (lowermost spectra) and ending in the interior of the fiber (uppermost spectra). One should bear in mind that this type of analysis is limited to nonpigmented hair fibers as melanin absorbs incoming laser light and interferes with Raman emission. Regardless, examples of spectra obtained from two Raman regions, 400 to 1750 cm^{-1} and 2800 to 3020 cm^{-1}, are shown in Figure 8. Going from the hair surface to the medulla (see Figures 12A and 12B) the bands at 1080, 1125, 1295, 2848, and 2878 cm^{-1} increase in intensity indicating higher levels of lipid in the interior of the fiber. The bands at 1295, 2848, and 2878 cm^{-1} are a result of C–H twisting, symmetric stretching, and asymmetric stretching vibrations of lipid methylene groups, respectively. The band at 2934 cm^{-1} is assigned to C–H symmetric stretching in pendant methyl groups in proteins (i.e., amino acid side chains). Taking the peak intensity ratio of the bands at 2848–2934 cm^{-1} allows for the calculation of the level of lipid relative to protein present in the sample. The bands at 1080 and 1125 cm^{-1} are due to C–C skeletal stretching in lipids. The peak intensity ratio of 1125 to 1080 cm^{-1} provides an indicator of lipid conformation order in the sample.

For better illustration, Figure 12C contains three spectra obtained from various depths within the fiber (cuticle, cortex, and medulla) in the 1200–1750 cm^{-1} region. An amide

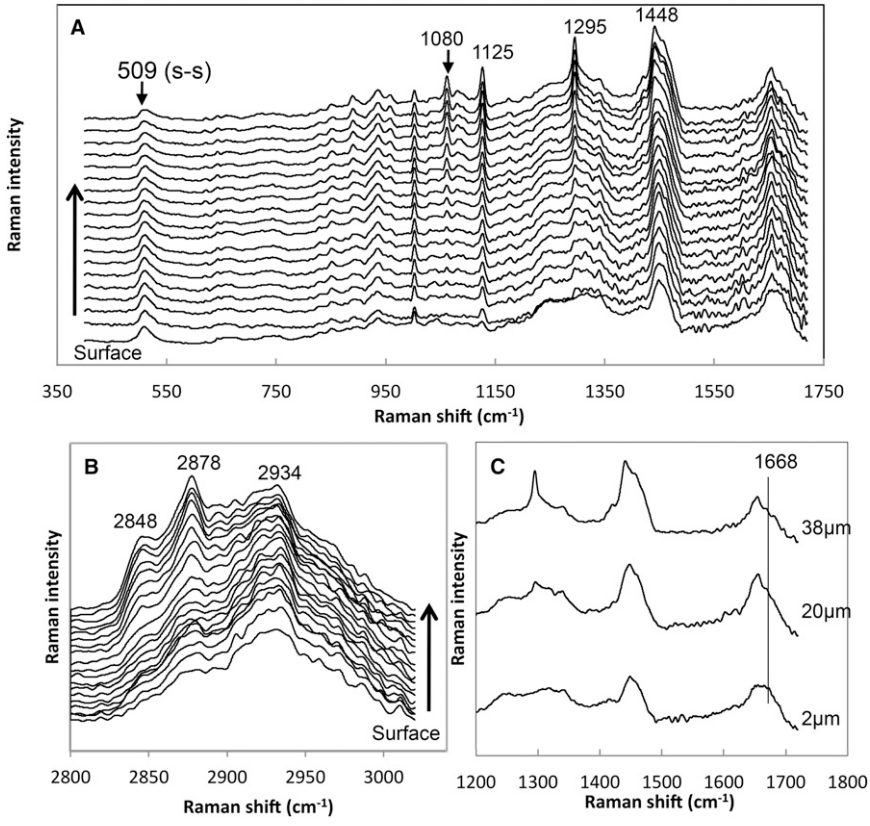

Figure 12. Raman spectra of untreated non-pigmented white hair. Spectra in (A) and (B) were obtained by depth profiling beginning at the surface of hair with the lower most spectrum and ending in the interior of the fiber with the uppermost spectrum. See text for peak assignments. The three spectra in (C) were obtained at various depths in the fiber and demonstrate a change in the shape of the amide band at 1668 cm^{-1} indicative of higher levels of beta conformation in the cuticular region. Originally published in Reference 25. Reprinted with permission of the Society of Photo Optical Instrumentation Engineers, Copyright 2011.

I band is present in the 1500–1720 cm^{-1} region and its frequency depends on the type of protein secondary structure. The band at 1668 cm^{-1} corresponds to beta sheet conformation. The width of this peak varies with depth in the fiber, being broader in the cuticle and sharper in the cortex. The band at 1685 cm^{-1} is associated with disordered protein structure.

The level of disulfide bonds can be monitored utilizing the peak data of the band at 509 cm^{-1}, which is due to S–S stretching. The relative amount of disulfide bond is calculated by taking the peak area ratio of 509 to 1448 cm^{-1} (due to C–H scissoring in CH_2 and CH_3 moieties) (25).

MONITORING THERMAL DAMAGE IN HAIR WITH RAMAN CONFOCAL IMAGING

Similar to FT-IR spectroscopic imaging, one may generate distribution maps of specific molecular species in a specimen with Raman confocal imaging. In addition to following changes in protein structure, the level of lipids and their degree of order can be

monitored. As an example of changes in hair as a result of treatment with a hot iron (230°C, 12 min; see explanation above for treatment protocol), Figure 13 contains Raman spectra for virgin and thermally treated hair. Immediately evident from the spectra is the decrease in intensity of the peak at 509 cm^{-1} corresponding to S–S stretching and the development (or an increase) of a peak at 487 cm^{-1}. This second peak (487 cm^{-1}) is believed to arise from an isomeric form of the S–S bond (30). It is likely that thermal treatment could result in transformation to other conformers of S–S, which could be associated with changes in the overall three-dimensional structure of the protein.

To gain a better perspective on the distribution of disulfide bonds in a cross section of hair, Figure 13 contains two depth profiling Raman images for virgin versus thermally treated hair from the exterior (0 μm) of the fiber to its interior (40 μm). These images were generated by taking the ratio of peak area at 509 cm^{-1} to 1004 cm^{-1} corresponding to phenylalanine present in the protein. On inspection of the images, it is immediately evident that virgin hair contains more disulfide bonds than thermally treated hair. Interestingly, we can see a distribution within virgin hair itself where the greatest amount of disulfide bonds is in the cuticle region (0–5 μm). It should be noted that in these experiments we do not obtain accurate readings from the other side of the fiber (>40 μm) due to signal decay with the laser. In addition to following the level of disulfide bonds, we can also look at the newly formed isomeric species by taking the ratio of the band at 487 cm^{-1} to the phenylalanine band (1004 cm^{-1}). Not surprisingly, the level of this species in virgin hair is extremely low (see Figure 13). In thermally treated hair, it appears that there are greater quantities in the internal portion (cortex) of the fiber and less present in the cuticle. Although this is in contrast with what one might expect,

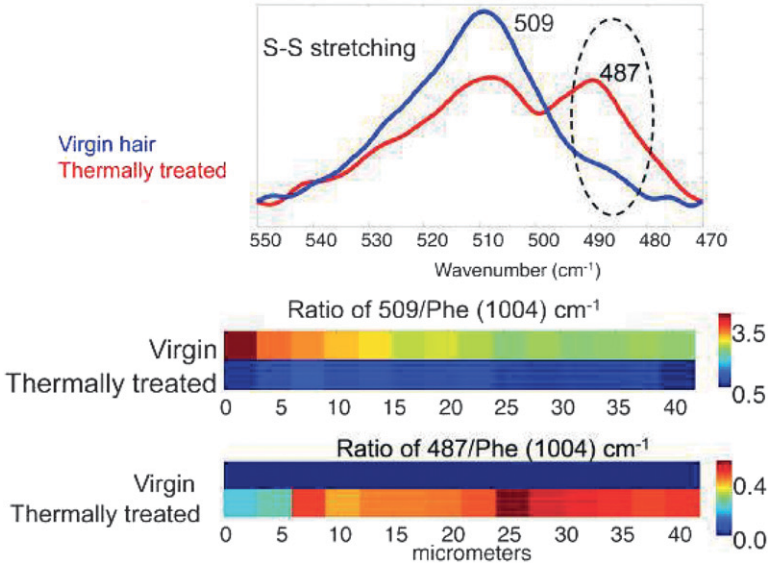

Figure 13. Raman spectra of virgin and thermally treated hair containing a normal S–S stretching band (509 cm^{-1}) and a possible isomer of S–S (487 cm^{-1}) resulting from thermal exposure. Raman depth profiling images provide spatial distribution maps of the natural S–S conformation and its damage-induced conformer in healthy and thermally treated hair. Images were normalized by taking the ratio of these bands to a protein phenylalanine band at 1004 cm^{-1}.

since the cuticle is the outermost structure of hair in contact with the hot iron, the cuticle cells may be more protected than the internal amorphous matrix. In unpublished studies, we examined cross sections of hair with scanning electron microscopy and found that while the cuticles appeared to have normal, healthy morphology, the cortical region contained numerous cavities where tissue was incinerated (see Figure 14). This leads us to believe that cuticle cells, protected by the highly cross-linked A-layer and exocuticle, are less prone to thermal damage than cortical cells residing in the interior of the fiber.

INFRARED THERMOGRAPHY TO IMAGE WATER IN THERMALLY TREATED HAIR

Infrared thermography (IRT) uses thermal imaging cameras that detect emitted radiation in the IR region of the electromagnetic spectrum. The usefulness of IRT in quantifying surface heat depends on the quasi-relationship between the emitted IR radiation (λ=3–15 cm^{-1}) and the magnitude of the surface temperature. Subsequently produced digital images, or thermograms, consist of two-dimensional image grids with temperature measurements plotted on a third axis using a relative color image scale.

BLACK BODY RADIATORS AND THE EMISSIVITY OF HUMAN HAIR

The Stefan–Boltzmann law ($Q = \varepsilon\sigma T^4$) relates the maximum achievable emissive radiation across all wavelengths, Q, to the fourth power of the absolute surface temperature, T, of a material, where σ is the Stefan–Boltzmann proportionality constant. For a solid black body radiator, Q reaches its maximum because the emissivity (ε) equals unity. The emissivity, which is a measure of the quantity of radiation a material emits from its surface relative to a black body, ranges from 0 to 1, where higher magnitudes are indicative of

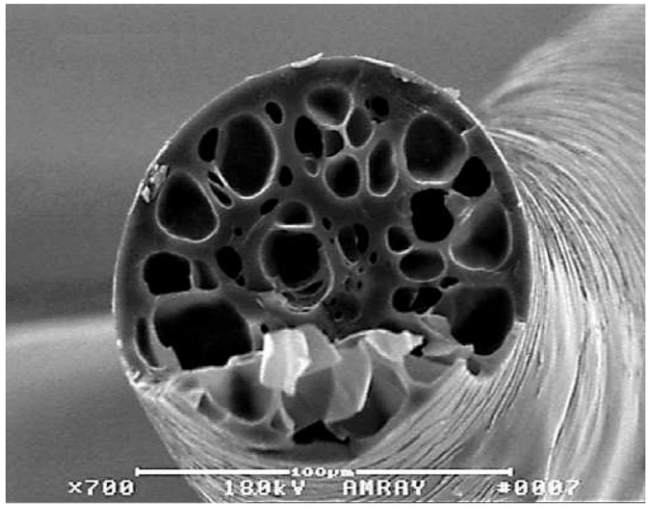

Figure 14. SEM micrograph of hair exposed to a curling iron at 230°C for 5 seconds illustrating the deleterious effects to the internal morphological components of hair.

more efficient radiators. For example, if you place a planar thermocouple on the surface of a sweltering asphalt tarmac (ε = 0.93) in mid-summer and then compare the reading to the radiative energy emitted across all emitted wavelengths, Q would virtually correlate with the fourth power of the measured absolute surface temperature of the solid. The human body is nearly a black body radiator, wherein the ε of water is 0.96–0.98, and the ε for human hair is 0.91 (31,32).

EFFECT OF FLAT-IRONING ON THE RADIATIVE PROPERTIES OF HUMAN HAIR

To gauge the impact of thermal insult on the radiative decay properties of human hair, a virgin hair tress, and an excessively flat-ironed hair tress (175°C, 0.6 in/min root-to-tip sweeps for 5 min) were simultaneously evaluated after exposure to a convective heat source. After a full day of equilibration at ambient conditions (32–35% RH; 20–22°C), to facilitate proper equilibration with ambient water vapor, the extended tresses were exposed to a portable space heater (75°C) that was positioned behind the tresses and powered on high for 5 min. The heater was then rapidly removed and an IR camera was used to immediately monitor the radiative emission of heat from the tresses as they cooled

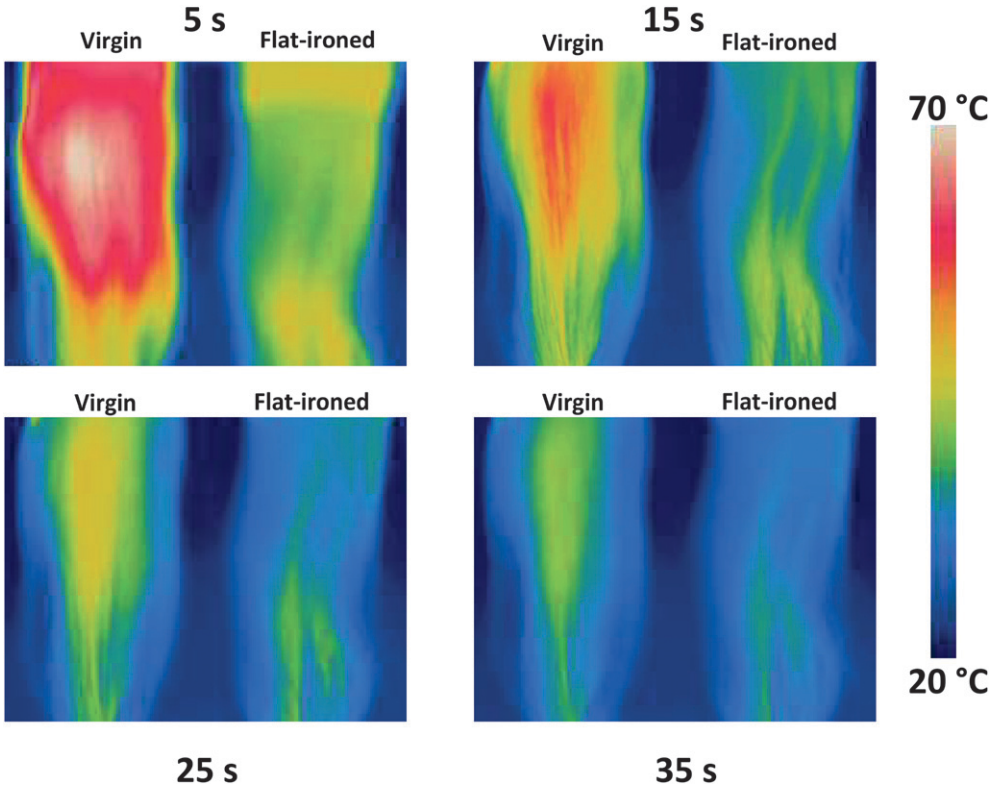

Figure 15. Series of thermal images indicating the kinetics of radiative heat dissipation. The tresses were equilibrated at 32–35 %RH for 24 hours prior to exposing to a 75°C convective heat source. Each image shows the states of the virgin (left) and hot flat-ironed virgin (right) European dark brown tresses. Images were logged every 10 s, starting at the 5 s mark, and clearly displays the decay of the virgin tress is slower than that of the thermally styled tress.

from approximately 70°C to ambient. Figure 15 captures the thermal decay as a series of sequential thermograms and clearly suggests that the virgin tress (left tress) cools to room temperature more slowly than the previously flat-ironed tress (right tress). Chemical changes that may be tied to the radiative differences are the formation of diisopeptide (amide) or lanthionine cross-links, where diisopeptide cross-linking has been reported to occur at approximately 165°C in keratin (33). Extensive amide cross-linking, via reactions between lysine and glutamic/aspartic acid (or their amides) may lead to a reduction in swell volume, thereby limiting the maximum water regain of thermally damaged fibers (29). Hence, one possible explanation for differences in the radiative decay rates for virgin and thermally damaged hair is that excessive thermal treatments rework the core fiber structure and, subsequently, the kinetics of the essential water-binding, hydrogen bonding, and thermal capacity systems of the hair.

DYNAMIC SCANNING CALORIMETRY TO MONITOR PROTEIN CHANGES IN THE AMORPHOUS AND CRYSTALLINE REGIONS OF HAIR

DSC facilitates an understanding of the physicochemical states of the crystalline intermediate filaments (IFs) and the amorphous matrix, or IF-associated proteins (IFAPs). In a DSC experiment, the influence of thermal energy on phase transitions, such as melting (T_m) or glass transition (T_g) events, is recorded as a function of applied temperature. Heating or cooling characteristic materials facilitates measurable variations in heat capacity (C_p), where ΔC_p may be monitored by recording excess, or differential, heat flow as a sample undergoes a phase, physical, or chemical transition. Depending on the thermal event, excess heat flows to the sample (endothermic), or from the sample (exothermic), relative to the empty sample pan. For example, glass transition (T_g) and melting (T_m) events are endothermic, whereas crystallization processes are exothermic.

EFFECT OF THERMAL STYLING ON THE DENATURATION TEMPERATURE OF THE IFS

Conveying excessive styling heat to a hair fiber aggravates the natural organizational structure of the cortex as thermally induced alterations in IFs-IFAPs covalent bonding and/or IFAPs cross-link density decrease the degree of alpha keratin crystallinity (34,35). The denaturation temperature (T_D) describes the thermal stability, and the position of T_D on the temperature scale is kinetically controlled by the cystine-based cross-link density and viscosity of the non-helical amorphous matrix (36). Further, the thermal energy, or enthalpy (ΔH_D), needed to unfold or denature the helix correlates with the structural rigidity of the alpha helices bound within the IFs (37). Physically speaking, DSC thermograms describe the denaturation of the secondary alpha-helical structure to random coils and beta domains via trends in the magnitudes of the endothermic denaturation temperature and enthalpy transitions.

HIGH-PRESSURE DSC ANALYSIS OF HAIR

In dry DSC methodology, hair is carefully cut into 1–2 mm pieces and then charged into "pinholed" aluminum DSC pans. During the experiment, water is evolved from the pan

as samples are heated to decomposition. Unfortunately, overlapping protein denaturation (T_D) and decomposition endotherms confound the results. The issue is overcome by presoaking the fiber snippets in water and subsequently charging into sealed stainless steel, high-pressure DSC capsules. By exploiting the water-plasticization behavior of the matrix, which shifts the hair denaturation peak from 230–250°C to 120–150°C, the T_D and pyrolysis events are opportunely resolved. More importantly, the area of ΔH_D is unaffected by prehydration, meaning that the extent of crystallinity is measurable since the helical structures are not tainted by excess water.

EFFECT OF THERMAL HISTORY ON THE EXTENT OF ALPHA KERATIN CRYSTALLINITY

As indicated in the trends in ΔH_D and T_D in the thermogram in Figure 16, the process of high-temperature flat ironing (232°C) affects the stability of the IFs. Diminishing magnitudes of ΔH_D, which is defined by the area of the endothermic DSC peak, result from prior exposure of the hair tress to the rigors of hot flat ironing. Changes in the denaturation enthalpy reveal that excessive temperatures influence the viscoelasticity of the amorphous matrix and subsequently destabilize the embedded alpha helices. In addition,

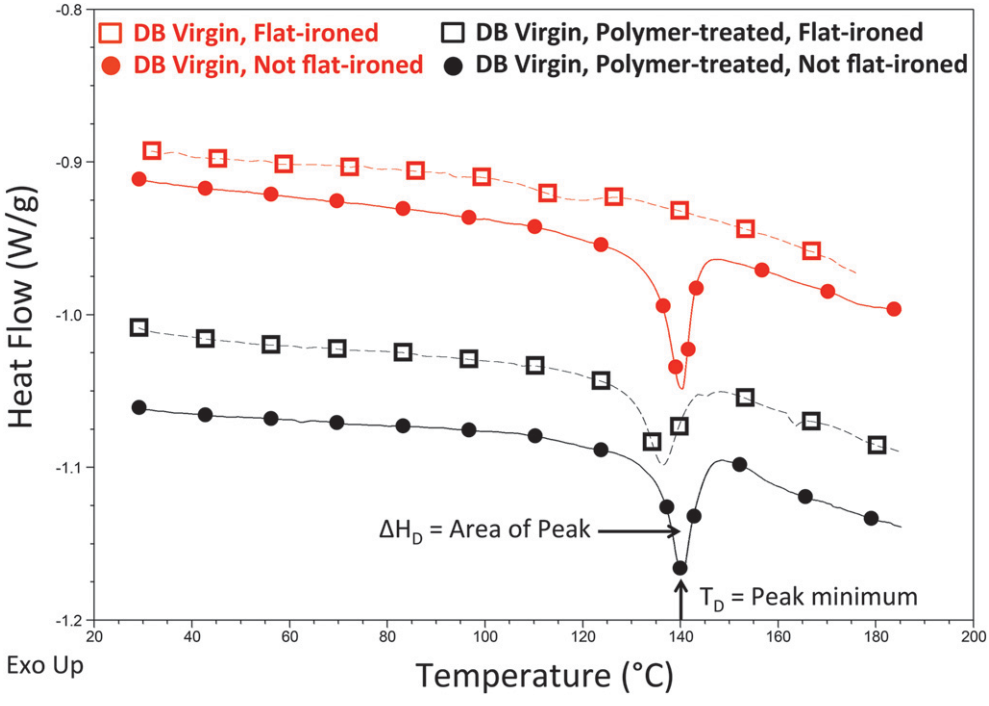

Figure 16. Overlay of HPDSC thermograms for virgin, thermally styled virgin, polymer-treated virgin, and thermally styled and polymer-treated virgin European dark brown hair assemblies. The top curve (open red squares) shows a very faint endothermic peak at ~115°C, whereas the untreated virgin sample (red circles) displays a characteristically sharp endotherm at 140°C. The bottom curves show the results of polymer-treated fibers, demonstrating that the protective polymer appears to preserve the endotherm for the heat-treated fibers (open black squares). The individual endotherms have been offset on the ordinate axis for visual clarity.

the diminution in T_D, which is marked by a shift to the left on the abscissa, is related to a decrease in the matrix cross-link density and/or scission of the nonhelical terminal domains of the IFs—where one functional culprit is an increase in the number of thermally induced disulfide bond scissions (35,38).

Figure 16 portrays a high-pressure DSC (HPDSC) overlay data for virgin, flat-ironed virgin, polymer-treated virgin, and polymer-treated and flat-ironed virgin European dark brown hair tresses. Relative to the characteristic endotherm for the untreated virgin fibers, the flat-ironed virgin thermogram demonstrates the deleterious consequences of thermal insult on the cortical proteins, wherein the profiles of ΔH_D and T_D are not apparent. Extending the technique to evaluating protective polymer treatments, samples represented by the bottom two curves were treated analogously, with the exception that each was also equivalently treated with poly(methylvinyl ether-*alt*-maleic anhydride) prior to challenging in HPDSC experiments (4.5 mg polymer/g hair). McMullen and Jachowicz had previously concluded that thermally styled fibers treated with poly(methylvinyl ether-*alt*-maleic anhydride) protected hair fibers against protein damage, as evidenced by the attenuation of tryptophan decomposition (39). In contrast to the untreated virgin and polymer-treated virgin samples, the flat-ironed and polymer-treated sample had a substantial ΔH_D peak and only a small shift in T_D; hence, the HPDSC results align with the protein-protective conclusions presented in the earlier fluorescence work.

TENSILE PROPERTIES OF HAIR

The mechanical strength of hair is one of its most important attributes. It describes the bending and/or tensile properties of hair, and is important not only for general hair health, but also plays a major role in hair's adaptability to grooming conditions. Hair strength is a term often used to describe the health state of hair when exposed to various stresses and strains. It can be weakened due to harsh cosmetic treatments, such as permanent waving, bleaching, and relaxing as well as exposure to UV radiation and physical insult with thermal styling appliances. Measurement of the tensile strength of hair specifically reflects the health state of the hair's innermost cortical cells that comprise the cortex (40). This is one of the most commonly used techniques in industry to assess damage incurred by treatments employed to change the shape of hair as well as protective effects afforded by hair protection agents. Therefore, in the remainder of this section, we will review the fundamental aspects of techniques to measure tensile properties and examine the influence of damaging and protective treatments.

MEASUREMENT OF TENSILE STRENGTH

Tensile strength measurements of hair are frequently carried out using an instrument equipped with a load cell that is able to monitor stress as a function of strain or vice versa. As illustrated in Figure 17, a fiber is mounted with crimps on both sides, which allows it to be grabbed by mechanical or pneumatic clamps. The instrument is programmed to deform the fiber along its longitudinal access by stretching the fiber at a programmed strain rate. Historically, instruments designed by Instron were used to carry out such

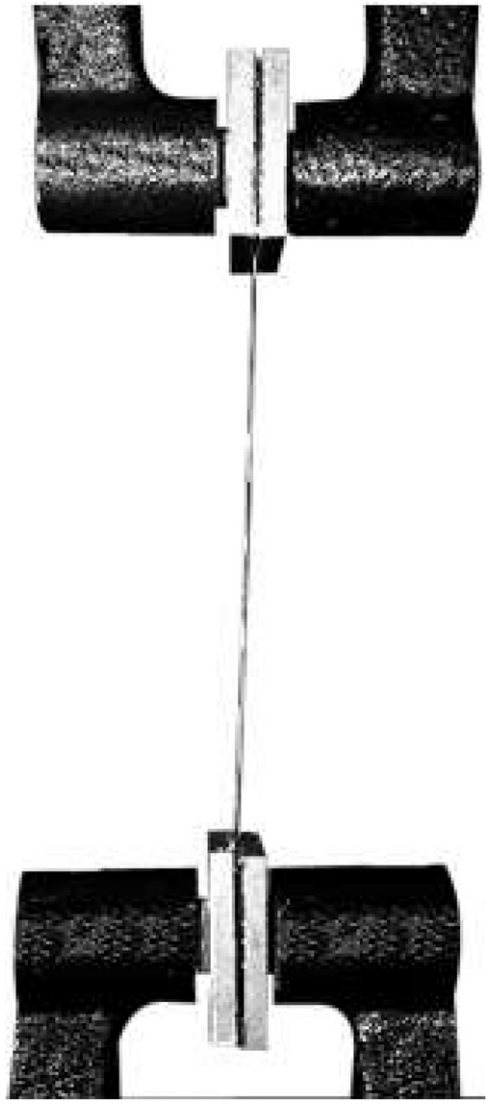

Figure 17. Photograph of pneumatic clamps of an Instron tensile tester containing a mounted hair fiber.

measurements. Similar studies can be carried out with a Texture Analyzer, manufactured by Stable Micro Systems, Ltd. In the late 1980s, Dia-Stron, Ltd., located in the United Kingdom, devised an instrument specifically designed to measure such properties of hair fibers. This same company has developed more advanced models over the years, which are capable of automation, a feature that is extremely useful since at least 100 fibers should be used for each data point to obtain good statistical significance. Moreover, to obtain key fiber properties such as the Young's modulus, it is necessary to know the cross-sectional area of each fiber. With the latest Dia-Stron instrumentation, such measurements are carried out in conjunction with a laser micrometer that measures the large (D_{max}) and small (D_{min}) axis diameter of elliptically and cylindrically shaped hair fibers. A common

parameter to characterize the shape of hair fibers is the *Elliptical ratio*, which is calculated from the diameter measurements:

$$Elliptical\ ratio = \frac{D_{max}}{D_{min}} \qquad (3)$$

The cross-sectional area of the fiber, used to calculate Young's modulus, is defined as the product of the radii from the two measurements:

$$A = \pi r_{\max} r_{\min} \qquad (4)$$

where A is the cross-sectional area of the fiber and $r_{\max}$ and $r_{\min}$ are the radii of the large and small fiber axes, respectively. After the fiber diameter is determined, tensile strength measurements may be carried out. There are several important parameters one should consider when conducting such experiments, such as the rate of strain during load elongation (the speed at which the fiber is extended), relative humidity, and the length of the fiber. Robbins cites relatively fast strain velocities used in his laboratory (0.05% strain per minute), which is extremely useful for carrying out screening studies, while Feughelman presents data gathered at really low strain rates (0.01% strain per minute), mostly for investigative purposes (41,42). Whichever velocity employed, we should be aware that strain rate will affect the magnitude of forces experienced by the fiber during load elongation. In addition, humidity will also influence the magnitude and shape of the stress–strain curve. Although most of this information is generally known, it would certainly be useful if there were more comprehensive studies on hair fibers in the literature demonstrating correlations in stress–strain behavior with these paramount variables carefully controlled.

INTERPRETATION OF STRESS–STRAIN CURVES

A typical stress–strain curve is provided in Figure 18 and demonstrates the difference in extensibility of the fiber at two different hydration levels. The plot is characterized by three different regions, which are indicated in the figure. First, at low strain (or low load elongation) the fiber undergoes a transition in the Hookean region. In this portion of the curve, the relationship between stress and strain is linear and one may calculate the elastic modulus (also referred to as Young's modulus) utilizing the following equation (41):

$$E = \frac{HgL}{A\Delta L} \qquad (5)$$

where H is the Hooken slope (g/cm), g is the gravitational constant (980.6 cm/s^2), L is the length of the fiber (cm), ΔL is the extension of the fiber, and A is the cross-sectional area of the fiber (cm^2). Traditionally, elastic moduli used to be reported in units of dynes/cm^2; however, the more modern practice incorporates the use of the SI system, utilizing units of N/m^2 or Pa.

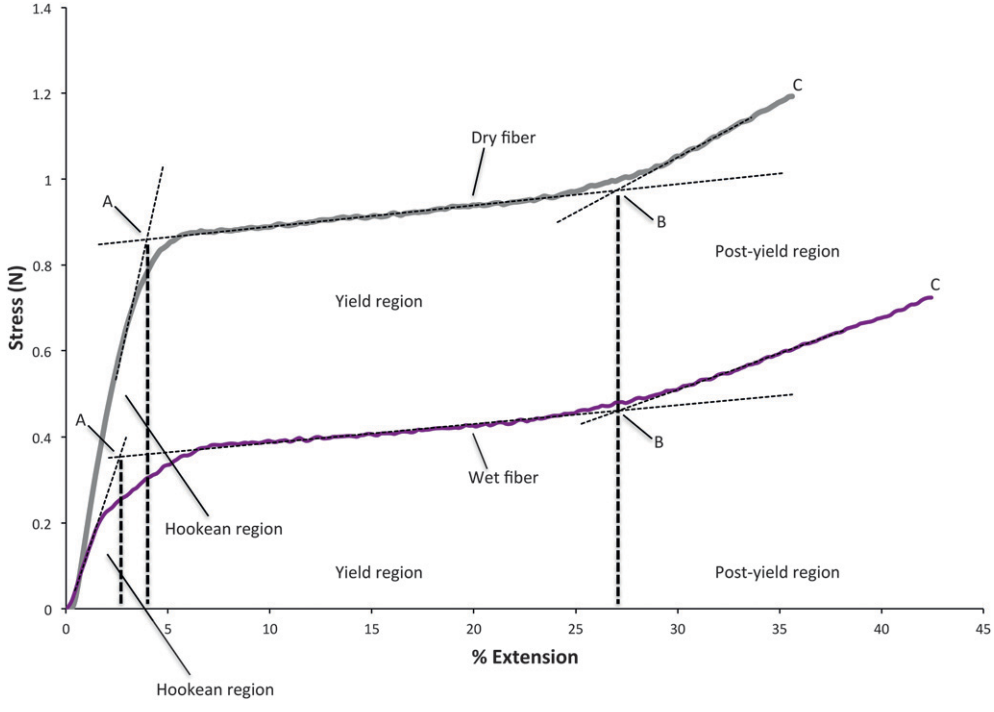

Figure 18. Illustrative load-elongation curves for dry and wet hair illustrating the different regions: Hookean, Yield, and Post-yield region. The end of the Hookean region is indicated by, A, the Hookean limit while the end of the Yield region is denoted by B, the Turnover point. The point at which the fiber breaks due to overwhelming strain is delineated by C.

Second, the end of the Hookean region is normally categorized by the Hookean limit, indicated by A on the chart. Third, the region between A and B is known as the yield region; and the end of the yield region (point B) is the turnover point. Fourth, the region bound by points B and C is the post-yield region. Finally, point C represents the force to break and the percent extension to break. One may also calculate the post-yield modulus, which is the slope of the stress–strain curve in the post-yield region.

As already noted, Figure 18 clearly demonstrates the influence of H_2O on the tensile properties of hair. The stresses in the load-elongation curve for hair containing greater amounts of water are much lower than that for a dryer hair sample. This phenomenon is due to the disruption by H_2O of hydrogen bonds and salt bridges that stabilize the alpha keratin structure, making the hair more extensible at lower applied forces. Not surprisingly, treatments that influence the chemical structure of hair will ultimately lead to greater/less H_2O sorption/desorption, thereby influencing the tensile properties of the fiber. It should be noted that in normal hair water can access the amorphous region, but is unable to ubiquitously penetrate the crystalline phase alpha keratin in normal, healthy hair.

In an extraordinary text written by Max Feughelman, entitled *Mechanical Properties and Structure of Alpha-keratin Fibres*, many of the fine details of wool structure are elucidated through interpretation of mechanical testing data (42). Feughelman demonstrates the utility of tensile strength studies to go beyond providing a simple measurement of fiber strength. He describes the cortex in terms of a simplified two-phase system—a crystalline

component composed of IFs embedded in an amorphous matrix of disulfide-rich globular proteins. During the extension of a keratin fiber, reversible and irreversible changes occur throughout the various phases of the stress–strain curve. For example, alpha keratin structure is conserved throughout the Hookean region. This means that the fiber can be extended up to the end of the Hookean region without inflicting permanent damage to the alpha keratin structure. Once we extend the fiber beyond the Hookean limit (A), conformational changes are introduced and alpha keratin is converted to beta keratin. Fortunately, this process is reversible throughout the yield region. Therefore, stretching a fiber up until the turnover point (B) will not lead to permanent changes in the crystal structure. It should be noted that approximately 30% of the alpha helix is converted to beta sheet in the yield region (42). When the alpha helix opens up, this changes the water management properties of hair—now, water can penetrate into the crystalline phase material. In the post-yield region, the fiber stiffens with increasing elongation. It is believed that disulfide cross-linking provides the major opposition force to extension in this region of the load–elongation curve. By this point, changes in protein secondary structure (conversion of alpha keratin to beta keratin) are permanent along with other major irreversible changes.

One should also bear in mind that tensile measurements performed on a virgin, undamaged fiber are much different than those completed on hair with a rich history of abuse. Further, conducting one load–elongation procedure (through the break point) is distinctive from a series of cycles carried out in the Hookean or yield regions (extension followed by returning to the state of origin). Such repetitive insult studies may offer a more realistic approach to mimicking hair's daily experience with brushing or combing. Alternatives to tensile strength measurements include mechanical fatigue and cyclical extension testing, which probably more accurately describe the forces encountered in daily grooming (41,43,44). Moreover, the forces generally encountered in tensile testing can often exceed that required to pull a fiber, including the follicle, from the scalp (45). Nevertheless, tensile testing provides us with greatly needed information on the overall physical condition of the fiber.

EFFECT OF DAMAGING TREATMENTS ON HAIR MECHANICAL PROPERTIES

A great deal of work has been conducted on the effects of bleaching and its influence on the tensile properties of hair. Robbins gives a review of this material where he outlines several important concepts (41). Findings suggest that wet tensile strength is more susceptible to bleaching than dry tensile strength. Bleaching damages disulfide bonds, converting cystine (disulfide bonds) to cysteic acid. More than likely, the hair fiber is more accessible by H_2O (especially in the matrix), in the absence of disulfide bonds, thereby disrupting hydrogen bonds and making the fiber more extensible (weaker tensile strength). We should also expect that the porous structure of bleached hair, due to decomposition of surface and internal lipids, might also play a role in facilitating H_2O access to the interior of the fiber. Likewise, a considerable amount of work has been completed to better understand the mechanical properties of permanently waved hair. Similar to the case of bleaching, permanent waving affects the dry tensile properties of hair less than the wet tensile properties. During the permanent waving process, disulfide bonds (cystine) in hair are reduced (cleaved), and then reformed by oxidative treatment

once the newly desired hair set is incorporated. This is not a high fidelity process, and the number of disulfide bonds reformed in the oxidation step does not reach the original number of disulfide linkages. Therefore, the internal structure of the fiber has more open channels/pathways for the incorporation of H_2O. Not surprisingly, wet tensile properties decrease after the reduction step and increase following oxidation—further evidence that demonstrates the role played by cystine (41). Furthermore, many lipids are also removed during permanent waving leading not only to a hair surface that is more porous/hydrophilic, but probably also a damaged cell membrane complex in the both the cuticle and cortex. The influence lipids have on tensile strength is not entirely clear. One study examined their effect on dry tensile strength and observed no difference in the tensile properties of virgin and solvent extracted hair (46). Unfortunately, these researchers did not conduct tensile strength studies in the wet state—information that would be extremely useful in light of the current discussion. Studies by Cheng and coworkers compared the effects of bleaching, permanent waving, and UV irradiation on tensile strength of hair and concluded that bleaching resulted in the most damage (47). This study compared the breaking load for the samples and is summarized in Table III. Such findings, while instructive, should be interpreted with caution as treatment protocols and experimental procedures may change from laboratory to laboratory. Unfortunately, there are no standard procedures for tensile testing—a technique used almost universally in the personal care industry.

Surprisingly, very little literature exists on the topic of tensile strength of hair that has undergone alkaline straightening procedures, such as relaxing (48). To achieve such geometrical changes in the shape of the fiber, hair is usually exposed to very high alkaline conditions brought about by treatment with either lye (NaOH) or non-lye (e.g., lithium hydroxide, calcium hydroxide) relaxers. In this manner, damage is indiscriminately done to both disulfide and peptide bonds. Unlike disulfide bonds, which are associated with changes in wet tensile strength, peptide bonds are believed to additionally influence dry tensile properties. With this line of reasoning, one would expect both the dry and wet tensile strength to decrease as a result of relaxer treatment (41). Unfortunately, only wet tensile data are available for chemically relaxed hair; until further studies are conducted we must wait with bated breath for complimentary dry tensile strength data. Table IV contains tensile strength data for chemically treated hair; again, providing evidence that bleaching results in the largest decrease in tensile strength.

Similar to the case of relaxing, very few studies have examined the effects of thermal treatment of hair in relation to its tensile properties (8,49). Contrary to expectations, there is a trend showing little change in the dry (65% RH) tensile properties of thermally exposed hair; and

Table III
Comparison of Different Chemical Treatments and Physical Insults to Hair and Their Influence on Tensile Properties (47)

Hair sample	Breaking load (N)
Untreated	94.13
UV irradiation	76.95 (96 h)
Bleaching	75.22 (12% H_2O_2)
Permanent waving	89.25 (pH 7) 78.53 (pH 9) 76.28 (pH 10)

Table IV
Tensile Strength Data for Chemically Treated Hair Measured in the Fully Hydrated State (48)

Hair sample	Tensile strength (N·m)/1000)
Untreated	1.21
Hair color (30 vol. developer)	1.14
Acid wave	0.99
Hair relaxer (NaOH)	0.78
Hair relaxer (guanidine)	0.70
Hair bleach (30 vol. developer)	0.48

even a slight increase in some of the tensile parameters. Similar to the case of wool, heating to elevated temperatures may result in the formation of cross-links within the internal structure of hair thereby requiring greater forces to extend and break the fiber (50).

CONCLUDING REMARKS

Chemical and physical treatments intended to change the shape of hair often result in changes to fiber shape, which is often accompanied by damage to structural proteins of the fiber. Photographic imaging techniques in conjunction with image analysis provide accurate measurements of fiber shape as manifested in fiber alignment and curl. In addition, using laser stereometry we characterize the three-dimensional structure of the fiber assembly and its occupied volume, allowing for comparison of the initial state with that of the reshaped hair. On the other hand, many other tools are available to assist in determining the location and extent of damage associated with reshaping hair. Spectroscopic techniques are the best tools at providing us with real chemical information as to the health state of hair. These changes can be probed by monitoring specific amino acid residues utilizing fluorescence spectroscopy, Raman spectroscopic imaging, or IR spectroscopic imaging. As an example, one may monitor tryptophan degradation with fluorescence, or conversion of cystine to cysteic acid residues by IR spectroscopic imaging. In all of the IR imaging data presented, we examined cross sections of hair fibers, providing specific chemical information in a spatially resolved manner. All of the spectroscopic techniques are advantageous; however, Raman confocal imaging is extremely powerful since it permits us to noninvasively dissect the fiber providing a z-line (through the fiber cross section) of functional group or secondary structure information. Both spectroscopic imaging methods also allow for the determination of beta keratin, and its localization in the morphological components of hair. In this way, we monitored the conversion of alpha keratin to beta keratin.

More common techniques to measure hair damage—especially due to perming, straightening, and flat ironing—include DSC and tensile property measurements. The increased utility of these techniques stems from their ease of use and instrument accessibility (e.g., budgetary factors). DSC provides us with a quick look at the health state of the crystalline (alpha-helical component) and amorphous (the matrix located in cortical cells) regions of hair by monitoring ΔH_D and T_D. Tensile strength measurements, on the other hand, are normally used to generate data about the tensile properties of hair. These data are typically presented in the form of stress–strain curves that provide a fingerprint of the

forces encountered when certain components of the crystalline phase are damaged; i.e., when alpha keratin is converted to beta keratin (yield region) or disulfide bonds are broken (postyield region).

ACKNOWLEDGEMENTS

The authors would like to express their gratitude to Dr. Trefor Evans of TRI-Princeton for his encouragement to write this article and to the management at Ashland Specialty Ingredients for their continued support of Research & Development in the area of hair care. Also, a great debt of gratitude is owed to Donald Koelmel for his contributions to the DSC section.

REFERENCES

(1) A. Byrd and L. Tharps, *Hair Story: Untangling the Roots of Black Hair in America* (Diane Pub Co., Collingdale, PA, 2006).
(2) A. Valdez, Brazilian hair straightening, *Cosmetiscope,* **17**(6), 1–7 (2011).
(3) R. McMullen, "Image analysis tools to quantify visual properties of hair fiber assemblies," in *Practical Modern Hair Science*, T. Evans and R. Wickett. Eds. (Allured: Carol Stream, IL, 2012), pp. 295–332.
(4) R. Asquith M. S. Otterburn, and J. A. Swift, Physical changes occurring in heated mammalian keratin, *J. Text. Inst.,* **63,** 544–550 (1972).
(5) I. Watt, Properties of wool fibers heated to temperatures above 100°C, *Text. Res. J.,* **45,** 728–735 (1975).
(6) M. Gamez-Garcia, The cracking of human hair cuticles by cyclical thermal stresses, *J. Cosmet. Sci.,* **49,** 141–153 (1998).
(7) R. McMullen and J. Jachowicz, Thermal degradation of hair. I. Effect of curling irons, *J. Cosmet. Sci.,* **49,** 223–244 (1998).
(8) S. Ruetsch and Y. Kamath, Effects of thermal treatments with a curling iron on hair fiber, *J. Cosmet. Sci.,* **55,** 13–27 (2004).
(9) T. Inoue, M. Ito, and K. Kizawa, Labile proteins accumulated in damaged hair upon permanent waving and bleaching treatments, *J. Cosmet. Sci.,* **53,** 337–344 (2002).
(10) M. Wong, G. Wis-Surel, J. Epps, Mechanism of hair straightening, *J. Cosmet. Sci.,* **45,** 347-352 (1994).
(11) J. Russ, *The Image Processing Handbook, 4th Ed.* (CRC Press: Boca Raton, FL, 2002).
(12) B. Pourdeyhimi and H. S. Kim, Measuring fiber orientation in nonwovens: The Hough transform, *Text. Res. J.,* **72,** 803–809 (2002).
(13) G. Loussouarn, A. Garcel, I. Lozano, C. Collaudin, C. Porter, S. Panhard, D. Saint-Léger, and R. de La Mettrie, Worldwide diversity of hair curliness: A new method of assessment, *Int. J. Dermat.,* **46** (Suppl. 1), 2–6 (2007).
(14) R. McMullen, F. Zisa, and J. Jachowicz, Measurements of hair volume by laser stereometry, *J. Cosmet. Sci.,* **60,** 171–185 (2009).
(15) J. Jachowicz and R. McMullen, Tryptophan fluorescence in hair—examination of contributing factors, *J. Cosmet. Sci.,* **62,** 291–304 (2011).
(16) S. Daly, R. Bianchini, T. Polefka, L. Jumbelic, and J. Jachowicz, Fluorescence and coloration of grey hair, *Int. J. Cosmet. Sci.,* **31,** 347–359 (2009).
(17) J. Prompers C. W. Hilbers, and H. A. M. Pepermans, Tryptophan mediated photoreduction of disulphide bond causes unusual fluorescence behavior of *Fusarium Solani pisi cutinase*, *FEBS Lett.,* **45,** 409–416 (1999).
(18) G. Zhang, D. J. Moore, R. Mendelsohn, and C.R. Flach, Vibrational microspectroscopy and imaging of molecular composition and structure during human corneocyte maturation, *J. Invest. Dermatol.,* **126,** 1088–1094 (2006).
(19) X. Bi, X. Yang, M. P. Bostrom, and N. P. Camacho, Fourier transform infrared imaging spectroscopy investigations in the pathogenesis and repair of cartilage, *Biochim. Biophys. Acta,* **1758,** 934–941 (2006).
(20) G. Zhang, D. J. Moore, C. R. Flach, and R. Mendelsohn, Vibrational microscopy and imaging of skin: from single cells to intact tissue, *Anal. Bioanal. Chem.,* **387,** 1591–1599 (2007).

(21) K. L. A. Chan, G. Zhang, M. Tomic-Canic, O. Stojadinovic, B. Lee, C.R. Flach, and R. Mendelsohn, A coordinated approach to cutaneous wound healing: vibrational microscopy and molecular biology, *J. Cell. Mol. Med.,* **12,** 2145–2154 (2008).
(22) J. Strassburger and M. Breuer, Quantitative Fourier transform infrared spectroscopy of oxidized hair, *J. Soc. Cosmet. Chem.,* **36,** 61–74 (1985).
(23) P. Dumas and L. Miller, The use of synchrotron infrared microspectroscopy in biological and biomedical investigations, *Vib. Spectrosc.,* **32,** 3–21 (2003).
(24) K. L. A. Chan, S. G. Kazarian, A. Mavraki, and D.R. Williams, Fourier transform infrared imaging of human hair with a high spatial resolution without the use of a synchrotron, *Appl. Spectrosc.,* **59,** 149–155 (2005).
(25) G. Zhang, L. Senak, and D. J. Moore, Measuring changes in chemistry, composition, and molecular structure within hair fibers by infrared and Raman spectroscopic imaging, *J. Biomed. Opt.,* **16,** 056009 (2011).
(26) R. Oertel, Protein conformational changes induced in human stratum corneum by organic sulfoxides: an infrared spectroscopic investigation, *Biopolymers,* **16,** 2329–2345 (1977).
(27) R. Mendelsohn and H. Mantsch, "Fourier transform infrared studies of lipid-protein interaction." in *Progress in Protein Lipid Interaction*, A. Watts and J. de Pont. Eds. (Elsevier, Amsterdam, 1986), Vol. 2, pp. 103–146.
(28) F.-J. Wortmann, M. Stapels, R. Elliot, and L. Chandra, The effect of water on the glass transition of human hair, *Biopolymers,* **81,** 371–375 (2006).
(29) Y. Zhou, R. Rigoletto, D. Koelmel, G. Zhang, T. W. Gillece, L. Foltis, D. J. Moore, X. Qu, and C. Sun, The effect of various cosmetic pretreatments on protecting hair from thermal damage by hot flat ironing, *J. Cosmet. Sci.,* **62,** 265–282 (2011).
(30) Z. Wen, Raman spectroscopy of protein pharmaceuticals, *J. Pharm. Sci.,* **96,** 2861–2878 (2007).
(31) FLIR Systems. *FLIR User's Manual* (2011).
(32) J.A. Preciado, B. Rubinsky, D. Otten, B. Nelson, M. C. Martin, and R. Greif, Radiative properties of polar bear hair, *Adv. Bioeng.,* **53,** 1–2 (2002).
(33) I. Rusznak, L. Trezl, A. Bereck, and G. Bidlo, Influence of short thermal treatments on wool, *Appl. Polymer Symp.,* **18,** 175–183 (1971).
(34) F.-J. Wortmann and H. Deutz, Characterizing keratins using high-pressure differential scanning calorimetry, *J. Appl. Polym. Sci.,* **48,** 137–150 (1993).
(35) D. Istrate, C. Popescu, and M. Möller, Non-isothermal kinetics of hard alpha-keratin thermal denaturation, *Macromol. Biosci.,* **9,** 805–812 (2009).
(36) J. Marsh, C. J. Clark, K. Meinkert, and R. M. Dahlgren, High-pressure differential scanning calorimetry of colorant products, *J. Cosmet. Sci.,* **58,** 621–627 (2007).
(37) F.-J. Wortmann, G. Wortmann, J. Marsh, and K. Meinkert, Thermal denaturation and structural changes of alpha-helical proteins in keratins, *J. Struct. Biol.,* **177,** 553–560 (2012).
(38) A. Dussaud, B. Rhana, and H. T. Lam, Progressive hair straightening using an automated flat-iron: function of silicones, *J. Cosmet. Sci.,* **64,** 119–131 (2013).
(39) R. McMullen and J. Jachowicz, US Patent 6,241,977 (2001).
(40) C. Robbins and R. Crawford, Cuticle damage and the tensile properties of human hair, *J. Soc. Cosmet. Chem.,* **42,** 59–67 (1991).
(41) C. Robbins, *Chemical and Physical Behavior of Human Hair, 5th Ed.* (Springer: Heidelberg, 2012).
(42) M. Feughelman, *Mechanical Properties and Structure of Alpha-Keratin Fibres: Wool, Human Hair, and Related Fibres* (UNSW Press: Sydney, 1997).
(43) M. Gamez-Garcia, Cuticle decementation and cuticle buckling produced by Poisson contraction on the cuticular envelope of human hair, *J. Cosmet. Sci.,* **49,** 213–222 (1998).
(44) Y. Kamath, S. B. Hornby, and H.-D. Weigmann, Mechanical and fractographic behavior of negroid hair, *J. Soc. Cosmet. Chem.,* **35,** 21–43 (1984).
(45) M. D. Berthiaume, D. A. Riccio, and J. H. Merrifield, Silicone based products for damaged hair in various ethnic groups, *Drug Cosmet. Ind.,* **155**(6), 24–32 (1994).
(46) R. L. McMullen, D. Laura, S. Chen, D. Koelmel, G. Zhang, and T. Gillece, Determination of physicochemical properties of delipidized hair, *J. Cosmet. Sci.,* **64,** 355–370 (2013).
(47) S. Cheng, C. W. M. Yuen, C. W. Kan, and K. K. L. Cheuk, Analysis of keratin fibre damage under various surface treatment conditions, *RJTA,* **12,** 53–62 (2008).
(48) A. Syed and H. Ayoub, Correlating porosity and tensile strength of chemically modified hair, *Cosmet. & Toil.,* **117**(11), 57–64 (2002).
(49) P. Christian, N. Winsey, M. Whatmough, and P. A. Cornwell, The effects of water on heat-styling damage, *J. Cosmet. Sci.,* **62,** 15–27 (2011).
(50) E. Menefee and G. Yee, Thermally induced structural changes in wool, *Text. Res. J.,* **35,** 801–812 (1965).